ACS APPLIED MATERIALS & INTERFACES

RESEARCH ARTICLE

www.acsami.org

Honeycomb-Structured Films by Multifunctional Amphiphilic Biodegradable Copolymers: Surface Morphology Control and Biomedical Application as Scaffolds for Cell Growth

Yingdan Zhu, Ruilong Sheng, Ting Luo, Hui Li, Jingjing Sun, Shengdian Chen, Wenyan Sun, and Amin Cao*

Laboratory for Polymer Materials, Shanghai Institute of Organic Chemistry, Chinese Academy of Sciences, 345 Lingling Road, Shanghai 200032, China

Supporting Information

ABSTRACT: Recently, fabrication of functional porous polymer films with patterned surface structures at the scale from nanometer to micrometer has been attracting increasing interests in material science and nanobiotechnology. In this work, we present new preparation of two series of multifunctional amphiphilic copolymers and preparation of their microporous thin films on solid substrates. First, diblock dendritic poly(*l*-lysine)-*b*-poly(*l*-lactide)s and triblock dendritic poly(*l*-lysine)-*b*-poly(*l*-lactide)-*b*-dendritic poly(*l*-lysine)s (C1−C6) were synthesized through 4-dimethylaminopyridine (DMAP)-catalyzed living ring-opening polymerization of (*l*-)-lactide with (*l*-)-lysine dendron initiators, and their structures were characterized by nuclear magnetic resonance spectrometer (NMR), gel permeation chromatography (GPC) and matrix-assisted laser desorption/ionization Fourier-transformed mass spectra (MALDI-FTMS). Employing the breath-figure (BF) fabrication strategy, thin films of the synthesized amphiphiles (C1−C6) were drop-cast, and their surface topologies were examined by scanning electron microscopy (SEM) and atomic force microscopy (AFM), and the effects of new amphiphile structure and drop-casting parameters of amphiphile concentration, humidity and temperature on self-assembly of ordered porous surface were studied. Furthermore, the influence of surface energy of drop-casting substrates was additionally investigated. With a human cervical epithelial carcinoma cell line (HeLa), cytotoxicity of the prepared honeycomb-structured films by new amphiphile C6 was evaluated by thiazoyl-blue-tetrazolium-bromide (MTT) assay, and HeLa cell growth behavior with microporous amphiphile films as the scaffolds was also examined. It was found that tunable micropore diameter sizes and well ordered surface topologies of BF films could be achieved for the new prepared amphiphiles, and utilization of the honeycomb-like microporous films as scaffolds indicated favorable enhancement in cell proliferation. Therefore, the honeycomb-structured films by these biocompatible multifunctional amphiphiles may provide new materials as 3D-scaffold materials for potential application in tissue engineering and regeneration.

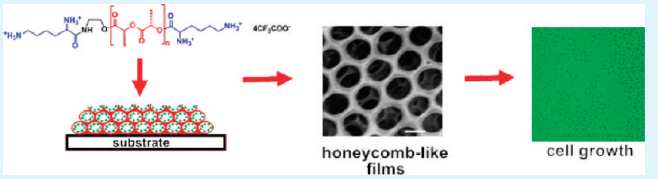

KEYWORDS: amphiphile, honeycomb structure, Breath-Figure method, porous film, cell scaffold

INTRODUCTION

Nano- and microstructured membranes, films, and monoliths have been becoming attractive due to a wide variety of potential and realized applications in microelectronics,[1,2] photonics,[3] picoliter beakers,[4] soft lithography,[5] templates,[6] catalyst supports,[7] optical materials,[8,9] superhydrophobic surfaces,[10−12] and so forth. Recently, the exploitation of honeycomb-structured films with highly ordered two- and/or three-dimensional patterns at the micrometer scale has raised great interests in biological applications such as separators,[13] templates for fabricating patterned proteins[14,15] or carbohydrates,[16] artificial organs, tissue regeneration scaffolds,[17−21] and so on. It has been found that the surface properties of a 2D monolayered or 3D multilayered polymer scaffolds played crucial roles in cell cultivation such as surface adhesion, spreading, migration, proliferation and differentiation,[22,23] and cell proliferation and surface adhesion on honeycomb-structured microporous films were revealed to be greatly influenced by the pore size.[24] In addition, cell signaling was more effectively activated on a honeycomb-structured microporous polymer film than on a flat counterpart.[22]

So far, to fabricate functional micro/nanoporous films with highly ordered pattern structures, a top-down template strategy has already been established and often exploited, involving a process of molding, direct writing, photolithography, colloidal crystal self-assembly and surface modification,[25] and sacrificed templates have been frequently utilized.[26−28] In the recent decades, a bottom-up templating strategy termed as breath-figure (BF) emerged, and becomes an important alternative way to fabricate honeycomb-structured films at micro/nanoscale. Since first being discovered in 1994,[29] BF has attracted increasing attentions for its superiority in many aspects: facile manipulation, low cost, solid mechanism of pattern formation, applicability for large-area fabrication and utilization of water as green medium.[27] In particular, the regularity of pattern and average pore size of porous polymer film could readily be tailored through finely tuning

Received: March 24, 2011
Accepted: June 23, 2011
Published: June 23, 2011

the BF fabrication conditions like polymer structures, concentration, solvent, substrate, gas flow, temperature, humidity, etc.[30−33] With regard to the self-assembly in bulk and/or at the interface, the chemical structure and architecture of a polymer have been found to greatly affect the consequent aggregate morphology at the scale across nanometer to macron,[34,35] and a variety of functional polymers have recently been utilized to prepare highly ordered nanoporous or microporous films via their corresponding BF stratigies,[15,18,19,31,36−46] and the average pore sizes were found to determine their possible applications from biomaterials to photonics.[27,33] For instance, star-shaped poly(styrene)s and poly(styrene)-*b*-poly(paraphenylene) block copolymers have been first reported to form honeycomb-like polymer films.[29] Recently Stenzel et al disclosed functional BF films prepared by amphiphilic diblock copolymer of poly(styrene)-*b*-poly(acrylic acid) (PS-PAA) for protein patterning templates.[15] Utilizing a triblock poly(styrene)-*b*-poly(butadiene)-*b*-poly(styrene) (SBS), Li and Ma et al.[19] prepared honeycomb-like films with uniform pore-size, topology and surface hydrophilicity after UV-light oxidation and successive cross-linking, and continuously examined their potential use as cell growth scaffolds. Kabuto et al[40] also revealed that a chemical cross-linking of BF films by poly(styrene-*co*-maleic anhydride) could greatly improve their thermal stability and solvent-resistance. Alternatively, with hyperbranched amphiphilic PAMAMs, Yan et al.[41] prepared highly ordered fluorescent honeycomb-patterned films with multilayered microstructures. Most recently, interesting photochromic metal-absorbing and multicolor luminescent ordered microporous films were separately fabricated from spiropyran polymers and new star-shaped polymers with styrene-fluorene conjugated moieties, and the formation of ordered microporous films was found to strongly depend on the molecular weights of star-shaped polymers.[47,48] In an overall view, since the discovery of BF methods for preparing porous polymer films with highly ordered patterns, poly(styrene) and poly(styrene)-based copolymers have often been applied. However, for further expanding the potential biomedical application, chemical structure, and biocompatibility of the polymer and as-fabricated BF films seem extremely important for their real applications in vitro and/or in vivo,[49] and highly ordered porous films with tunable pore sizes and surface topologies which can be prepared by a biodegradable and biocompatible polymer, seem to be favorable and practically demanded for diverse biomedical applications. Up to date, poly(*l*-lactide) PLLA which can be derived from a plenty of renewable natural sources, has been wildly explored as a promising biodegradable and bioresorbable material for tissue engineering;[50] however, to the best of our knowledge, only very few studies have been reported concerning the utilization of PLLA for successful BF fabrication of ordered biodegradable porous films.[24,38,51−55] It has also been revealed that pure hydrophobic PLLA seems to be difficult for preparing ordered microporous films unless some organic surfactants,[24,54] specific amphiphilic copolymers[20] or functional nanoparticles[38] were additionally utilized. On the other hand, it can be anticipated that the functional surfaces and interfaces of porous films would be lack of favorable functional groups for postmodification even though the well-ordered BF films could be prepared by pure PLLA. Hence, to explore new functional biocompatible polymers seems meaningful and important for facile preparation of well-ordered mesoporous films with functional groups at the interfaces and micrometer pore sizes for future biomedical applications.

In our previous works, we have successfully developed a metal-free synthetic strategy for preparing structurally well-defined biocompatible amphiphilic dendritic poly(*l*-lysine)-*b*-poly(*l*-lactide)s and dendritic poly(*l*-lysine)-*b*-poly(*l*-lactide)-*b*-dendritic poly(*l*-lysine)s from natural products of (*l*-)-lactic acid and (*l*-)-lysine,[56−59] and these new copolymer amphiphiles were further revealed to be highly biocompatible and able to efficiently bind and deliver plasmid DNA into cells.[57−59] In order to further explore their structure dependence of possible surfactant-free self-assembly of ordered honeycomb-like microporous films, in this work, new series of diblock and triblock copolymer amphiphiles were synthesized and characterized. Subsequently, the chemical structure and BF fabrication condition parameter dependences of physical properties of the prepared mesoporous polymer films were examined by scanning electronic microscopy, atomic force microscopy and dynamic contact angle testing instrument. Moreover, in vitro cell toxicity of these new synthesized amphiphile films was assayed by MTT with HeLa cells (a human cervical epithelial carcinoma cell line). Finally, HeLa cell growth on the prepared honeycomb-structured porous films as the scaffold was studied with nonporous flat films as the control, and was discussed.

EXPERIMENTAL SECTION

Materials. In this study, the monomer of (*l*-)-lactide (99%) was commercially supplied by Tokyo Kasei Inc. (Tokyo, Japan), and was further purified with repeated recrystallization in ethyl acetate. 2-aminoethanol (98%) purchased from Shanghai Lingfeng Chemical Reagent Co. Ltd. was freshly distilled prior to use. Boc_2O anhydride (99.0%), L-lysine (99.0%), diisopropyl ethylamine (DIEA), 1-hydroxybenzotriazole (HOBT) and 4-dimethylaminopyridine (DMAP) were all supplied by GL Biochem (Shanghai, China). *p*-Toluenesulfonic acid was purchased from Shanghai Sanpu Chemicals Co. Ltd. *N*,*N*′-Dicyclohexylcarbodiimide (99%) (DCC) and *N*,*N*′-diisopropylcarbodiimide (99%) (DIC) were bought from Shanghai Tianlian Fine Chemicals Co. Ltd. and Shanghai Medpep Co. Ltd., respectively. Trifluoroacetic acid (TFA, 97.0%) was purchased from Shanghai Sinopharm Chemical Reagent Co. Ltd. Solvent of chloroform was in turn washed by sulfuric acid, and then dehydrated over CaH_2 for 24 h and distilled before use. Moreover, paraformaldehyde (>95%) and thiazoyl-blue-tetrazolium-bromide (MTT) were bought from Bio Basic Inc. (Markham, Canada), and Dulbecco's modified eagle medium (DMEM) was commercially supplied by Genom Biomedicine Co. Ltd. (Hangzhou, China). Fetus bovine serum (FBS) was purchased from Sijiqing Biological Engineering Material Co. Ltd. (Hangzhou, China). In addition, the other reagents and solvents were of analytical grade, and were utilized as received, and the silicon wafers (5×5 mm^2) as film substrate were purchased from Structure Probe Inc.(Canada), and were hereby preliminarily treated before use as described in detail in the Supporting Information.

Syntheses of Diblock Dendritic Poly(L-lysine)-*b*-poly(L-lactide) and Triblock Dendritic Poly(L-lysine)-*b*-poly(L-lactide)-*b*-dendritic Poly(L-lysine) Amphiphiles. As shown in scheme 1, two new series of diblock dendritic poly(L-lysine)-*b*-poly(L-lactide)s and triblock dendritic poly(L-lysine)-*b*-poly(L-lactide)-*b*-dendritic poly(L-lysine) amphiphiles, namely DL_m-PLLA and DL_1-PLLA-DL_1 bearing different generation of L-lysine dendrons (DL_m) and PLLA block chain lengths, were accordingly synthesized via a metal-free DMAP catalyzed living ring-opening polymerization of (L-lactide in chloroform as we have recently reported.[56−59] In brief, the amino-group Boc-protected synthetic precursors of either PDL_m-PLLA (S1−S3) or PDL_1-PLLA-PDL_1 (S4−S6) were first prepared. Then, utilizing TFA-mediated Boc-deprotection of the synthetic precursors (S1−S6) at ambient temperature in dichloromethane, diblock DL_m-PLLA (C1−C3) and triblock DL_1-$PLLA_n$-DL_1 (C4−C6) as shown in Scheme 1 were finally prepared with quantitative yields.

Scheme 1. Molecular Structures of Diblock Dendritic Poly(L-lysine)-*b*-poly(L-lactide) and Triblock Dendritic Poly(L-lysine)-*b*-poly(L-lactide)-*b*-dendritic Poly(L-lysine) Amphiphiles with Various PLL Dendritic Generations and Different PLLA Block Chain Lengths

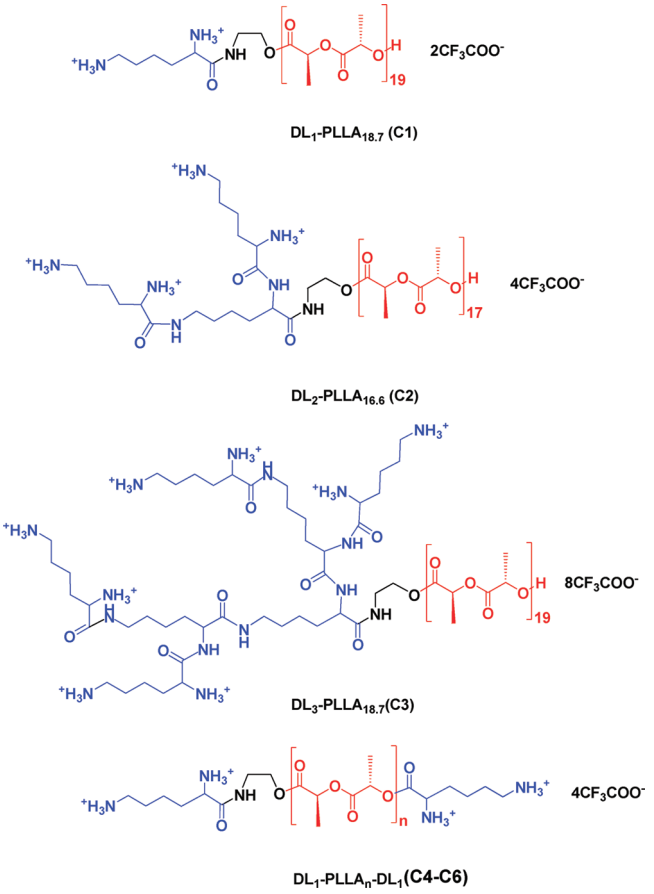

Preparation of Honeycomb-like Porous Films by Multifunctional Copolymer Amphiphiles. Films of the diblock dendritic poly(L-lysine)-*b*-poly(L-lactide)s and triblock dendritic poly(L-lysine)-*b*-poly(L-lactide)-*b*-dendritic poly(L-lysine) amphiphiles were hereby prepared by a static BF method, which is simple, and could avoid uncertainties often happened in a typical dynamic BF process.[25] A predetermined amount of copolymer amphiphile was first weighted and added into an organic solvent, and stirred to achieve homogeneous mixture solution. Then, 200 μL of as-prepared amphiphile solution was allowed to drop and cast onto a solid substrate, and was further transferred into a thermostatted IG-400 humidic chamber (Yamato, Japan) under a preset temperature and relative humidity (RH%) and kept for at least 30 min. After the evaporation of organic solvent and water, opaque BF polymer film on the substrate was obtained for further characterization. In parallel, flat films without porous topology as controls were also prepared by spin-coating 200 μL of the same organic solution onto the substrate at ~1000 rpm using a KW-4A spin-coater (Chemat Technology, USA).

Analytical Procedure. *NMR.* Proton NMR spectra were recorded in deuterated chloroform solution on a Varian VXR-300 Fourier-transformed nuclear magnetic resonance spectrometer at the room temperature, operating at 300.0 MHz for ^{1}H nuclei. ^{1}H NMR spectra were averaged with resonance signal accumulation of at least 32 scans, and tetramethylsilane (TMS) was utilized as an internal chemical shift reference.

Mass Spectra. Matrix-assisted laser desorption/ionization Fourier-transformed mass spectra (MALDI-FTMS) were recorded on an IonSpec 4.7T spectrometer (IonSpec Inc., USA) for the synthesized diblock DL$_m$-PLLA and triblock DL$_1$-PLLA$_n$-DL$_1$ amphiphiles (C1−C6) for their molecular weight characterization.

Gel Permeation Chromatography. Measurements of average molecular weights (M_n, M_w) and polydispersity (M_w/M_n) of the synthetic Boc-protected precursors of diblock dendritic poly(L-lysine)-*b*-poly(L-lactide)s and triblock dendritic poly(L-lysine)-*b*-poly(L-lactide)-*b*-dendritic poly(L-lysine) amphiphiles (S1−S6) were conducted on a PL GPC-50 Plus GPC instrument (Varian, UK). Chloroform was employed as the eluent at a flow rate of 1.0 mL/min and a temperature of 40 °C with one RisiPore Guard column (50 × 7.5 mm^2) and two PLgel 5 μm mixed-D columns (300 × 7.5 mm) (Polymer Laboratories, UK). Real-time elution traces were acquired by a RI detector via an attached Cirrus GPC software. Furthermore, polystyrene standards (Polymer Laboratories, UK) were employed to generate GPC elution traces for molecular weight calibration.

Scanning Electron Microscopy. Surface topologies and section view of honeycomb like amphiphile films were examined at ambient temperature on a JSM-6390LV scanning electron microscopy (JEOL, Japan) at 10−30 kV accelerating voltage, and the film samples were gold-sputtered using a JEOL JFC-1600 autofine coater prior to SEM measurements.

Atomic Force Microscopy. Characterization of surface topology for the prepared microporous amphiphile films was also conducted at room temperature on a NanoScope IVa multimode atom force microscopy (Veeco Instrument, USA), operating in tapping mode with a scanning speed of 0.1 Hz/s. AFM images were recorded under a resolution of 256 × 256 data points with an Olympus AC160TS cantilever (stiffness of 42 N/m and resonance frequency of 300 kHz).

Dynamic Contact Angle and Surface Energy. Dynamic contact angles of pure water on the prepared BF film surface were measured at 25 °C on a KH-0601 optical contact angle testing instrument (Kangsente, Beijing), and each 1 μL of water droplet was injected onto the BF film surface, and dynamic contact angles were thus evaluated through a Dropshape software (Kruess, Germany). In addition, surface energy of the drop-casting substrates was evaluated via Owens−Wendt−Rabel−Kaelble method on the basis of contact angles separately measured with pure water and ethylene glycol through the Drop Shape software.

Cell Toxicity Assay. In vitro cell toxicities of the drop-cast honeycomb-structured polymer films were examined by MTT assay, and the pristine silicon wafer was employed as the control. All the samples were first in turn sterilized with ethanol (70%, v/v) and UV light radiation for 30 min before cell cultivation. Then, the samples were separately placed into 48-well microplates with 200 μL DMEM per well containing 10% FBS, continuously HeLa cells were seeded into the wells (1 × 10^4 cells/well), and incubated at 37 °C for 24 h with 5% CO_2. Thereafter, 40 μL of MTT (5.0 mg/mL) was added into each well and kept incubation for 4 h before the replacement with fresh medium containing DMSO (200 μL/well) to dissolve the formazan-crystal formed in living cells. Finally, in vitro cell viabilities were evaluated at λ = 490 nm with λ = 630 nm as the reference on an Elx-800 microplate reader (Biotek, USA).

Cell Growth with Porous Films As the Scaffolds. In this study, HeLa cells were applied to examine cell growth behavior with porous amphiphile BF films as the scaffolds. At first, the porous BF films with distinct average micropore sizes were prepared by drop-casting the C6 amphiphile solution in $CHCl_3$ on clean glass slides at 25 °C and 47 RH% under various amphiphile mass concentrations (0.05−0.80% w/v), and flat-surface films were in parallel prepared via spin-coating as the control. Subsequently, the microporous films drop-cast on substrates were sterilized in a way as aforementioned, and then were placed into 6-well microplates with 2 mL of DMEM medium in each well containing 10% FBS. HeLa cells were continuously seeded onto the film surfaces (1 × 10^5 cells/well), and kept incubation at 37 °C for 6 h under 5% CO_2.

Afterward, the films were transferred into new wells in a 6-well microplate with fresh DMEM medium containing 10% FBS. As a result, living HeLa cells were periodically imaged and recorded on a Nikon Ti microscopy, and the surface cell density in cells/cm^2 was further evaluated to examine the BF film scaffold structure dependence of HeLa cell growth behavior. In addition, after 72 h of cell cultivation, the living HeLa cells on film surface were fixed with paraformaldehyde (4%) for 10 min, and their morphologies were then investigated by SEM.

RESULTS AND DISCUSSION

Synthesis of Two New Series of Multifunctional DL$_m$-PLLA and DL$_1$-PLLA$_n$-DL$_1$. In order to examine the structure dependence of fabricating honeycomb-structured porous films by new synthesized amphiphiles, two series of diblock dendritic poly(L-lysine)-*b*-poly(L-lactide)s (C1−C3) and triblock dendritic poly(L-lysine)-*b*-poly(L-lactide)-*b*-dendritic poly(L-lysine)s (C4−C6) as shown in scheme 1 were designed and accordingly prepared in a way as we have recently reported.[56−59] In this work, the diblock amphiphiles C1−C3 were prepared to bear similar PLLA lengths but distinct generation of hydrophilic L-lysine dendrons for exploring the DL dendritic generation dependence of BF fabrication of solid thin films. In comparison, triblock C4−C6 end-capped with L-lysine were also synthesized with varying hydrophobic PLLA chain lengths. As a result, Figure 1 shows GPC traces for the terminal amino-group Boc-protected synthetic precursors denoted as PDL$_m$-PLLA and PDL$_1$-PLLA-PDL$_1$ (S1−S6), and symmetric GPC elution traces with narrow distribution and polydispersity indices (PDI) of 1.08−1.18 demonstrated successful synthesis of diblock and triblock precursors (S1−S6) with well-defined molecular structures and architectures. On the basis of ^{1}H NMR spectra,[56−59] degrees of polymerization (DP) for the PLLA block chains were further evaluated to be 18.7, 16.6, 18.7, 12.0, 16.1, and 37.7 for the samples S1−S6, respectively, and the characteristics of diblock and triblock precursors (S1−S6) are summarized in Table 1. Consequently, through an efficient TFA-mediated Boc-deprotection of the S1−S6 in CH_2Cl_2, two new series of amphiphilic C1−C6 were achieved almost with quantitative yields, and their molecular weights were further characterized by MALDI-FTMS as seen in Figure S2 of Supporting Information, confirming successful preparation of new diblock DL$_1$-PLLA$_{18.7}$ (C1), DL$_2$-PLLA$_{16.6}$ (C2), DL$_3$-PLLA$_{18.7}$ (C3) and triblock DL$_1$-PLLA$_{12.0}$-DL$_1$ (C4), DL$_1$-PLLA$_{16.1}$-DL$_1$ (C5), DL$_1$-PLLA$_{37.7}$-DL$_1$ (C6).

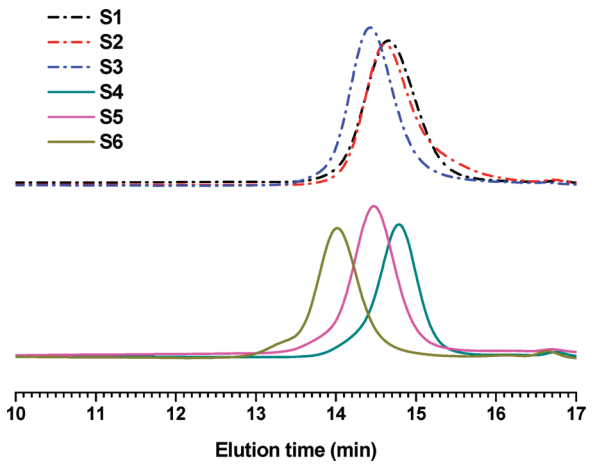

Figure 1. GPC traces for synthetic precursors of the amino Boc-protected PDL$_m$-PLLA (S1−S3) (upper) with various generation of L-lysine dendrons and PDL$_1$-PLLA$_n$-PDL$_1$ (S4−S6) (bottom) with different hydrophobic PLLA chain lengths.

Fabrication of Microporous BF Films by New Amphiphiles. In this study, microporous films of new synthesized amphiphiles were prepared in a way of static BF method, which has been reported to consist of multiple steps as illustrated in Scheme 2:[53,60−62] (A) First, copolymer amphiphile solution drop-cast on the substrate surface evaporated under humid environment; (B) then water droplets began to nucleate on the surface of evaporatively cooled solution, and were stabilized by the encapsulation of interfacial-attractive polymers; (C) the water droplet sizes grew larger by continuous uptake of moisture and/or possible water-droplet coalescence; (D) the water droplets eventually self-organized into hexagonal pattern driven by thermocapillary effects or Marangoni convection, and played as templates for subsequent copolymer amphiphile self-assembly; (E) finally, honeycomb-structured microporous amphiphile film was obtained after complete evaporation of organic solvent and water.

Since the discovery of fabricating ordered mesoporous films by BF method, a wide variety of functional polymers bearing different molecular structures and architectures have been reported to be capable of forming ordered BF films on diverse solid or liquid substrates,[15,18,19,31,40,43,45] and it has also been revealed that for an amphiphilic copolymer, the factor of its molecular hydrophobic/hydrophilic balance seemed to play an important role in final formation of ordered surface pattern of thin polymer

Table 1. Synthesis of the Amino Boc-Protected Dendritic Poly(L-lysine)-*b*-poly(L-lactide) and Dendritic Poly(L-lysine)-*b*-poly(L-lactide)-*b*-dendritic Poly(L-lysine) Precursors S1−S6

		molecular weight					
sample	structure	$M_{n,\ NMR}$[a] × 10^{-3}	M_w[b] × 10^{-3}	M_n[b] × 10^{-3}	M_w/M_n[b]	I_B/I_M[c]	DP of PLLA[d]
S1	PDL$_1$-PLLA$_{18.7}$	3.1	4.4	3.9	1.11	0.48	18.7
S2	PDL$_2$-PLLA$_{16.6}$	3.2	4.6	3.9	1.18	1.08	16.6
S3	PDL$_3$-PLLA$_{18.7}$	4.5	5.4	4.9	1.11	1.92	18.7
S4	PDL$_1$-PLLA$_{12.0}$-PDL$_1$	2.4	4.1	3.7	1.08	1.50	12.0
S5	PDL$_1$-PLLA$_{16.1}$-PDL$_1$	3.3	5.5	5.0	1.10	1.12	16.1
S6	PDL$_1$-PLLA$_{37.7}$-PDL$_1$	6.1	8.7	7.8	1.11	0.48	37.7

[a] Calculated as the sums of PLLA block and Boc-protected PLL dendrons. [b] Determined by means of GPC with polystyrene standards. [c] ^{1}H NMR intensity ratios of Boc methyl protons to PLLA methine protons; [d] Calculated in accordance with DP = 9.0 × 2^{m-1} × I_M/I_B for S1−S3 and DP = 9.0 × 2 × I_M/I_B for S4∼S6 (*m* denotes the generation of a PLL dendron).

Scheme 2. Self-Assembly of Microporous Structural BF Films by Drop-Casting PLLA-Based Block Amphiphile Solution on Solid Substrate

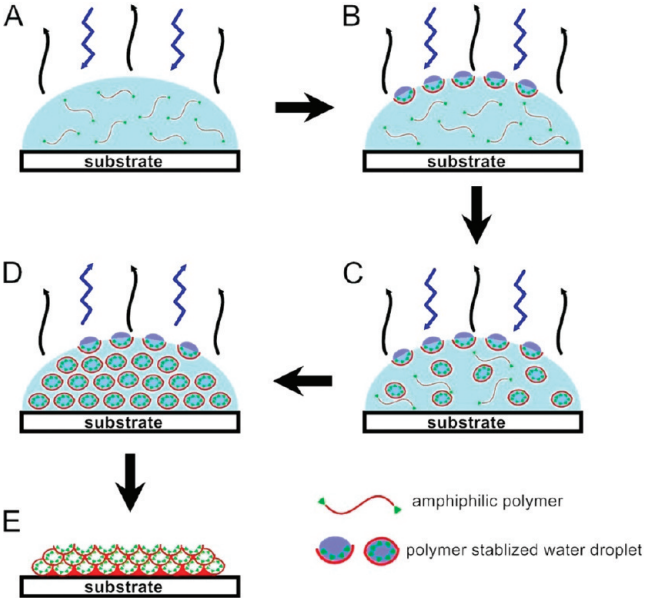

films.[60] Here, the two newly prepared series of copolymer amphiphiles were employed to examine their structure dependence of BF array (BFA) formation on solid substrates by drop-casting, and the SEM results are shown in Figure 2. It was revealed that the drop-cast films by diblock structural C1 and C3 nearly showed flat surface morphologies while the BF film by amphiphilic C2 with 2 generation PLL dendron exhibited microporous surface topologies even though the above three diblock amphiphiles have very similar PLLA chain lengths (DP = 17−19). Therefore, it could be inferred that the molecular hydrophilicity of the copolymer amphiphile played important roles in BF formation of ordered microporous surface. When increasing the hydrophilicity of a copolymer amphiphile, it could lead to more uptake of condensed water and increased water-droplet diameter sizes, thus decrease the template stability as ever been reported.[63,64] In contrast, when the amphiphile with low generation L-lysine dendron has low hydrophilicity, its inadequate capability to uptake condensed water droplets would also result in the formation of less stable template. In addition, it was interestingly noteworthy that the triblock C6 was observed to form ordered honeycomb-like film under the same drop-casting conditions even though its hydrophilic/hydrophobic block molar ratio is very close to that of diblock amphiphile C1, and this result indicated that the molecular architecture also influenced the thin BF film surface topologies. In view of Figure 2, the triblock C6 capable of forming a better ordered BF surface topology was further employed for exploring the casting parameter dependences of surface topologies of the self-assembled BF film.

To date, it has been reported that regularity and average pore size of the BF films were significantly influenced by the casting parameter of polymer concentration.[11,19,25] Figure 3 depicts the SEM surface topologies for the C6 cast on silicon wafer with $CHCl_3$ solvent under a series of mass concentrations of 0.05−1.60% w/v. It could be seen that under a polymer concentration of 0.05% w/v, monolayered microporous film surface formed

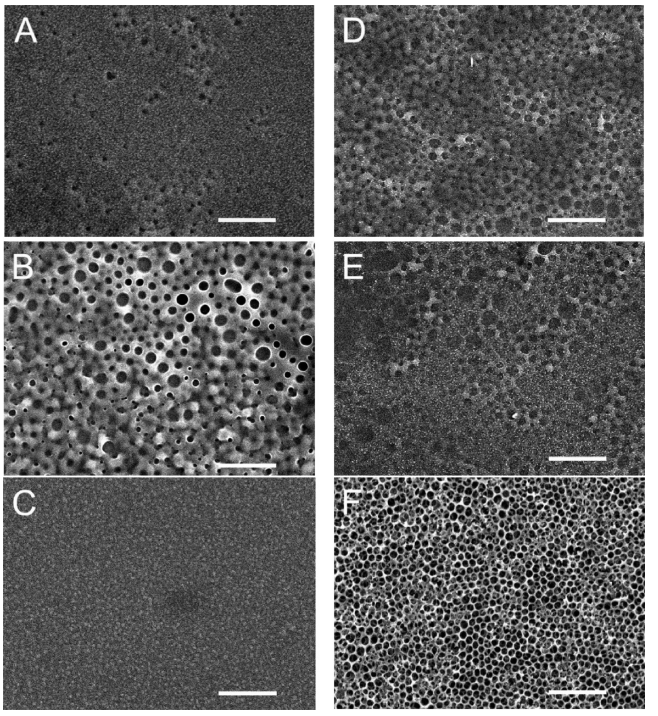

Figure 2. SEM images of the BF films drop-cast on pristine silicon wafer for diblock (A) C1, (B) C2, (C) C3, triblock (D) C4, (E) C5, and (F) C6 with $CHCl_3$ as organic solvent under amphiphile mass concentration of 0.40% w/v, 47 RH%, and 35 °C. Scale bar is 10 μm.

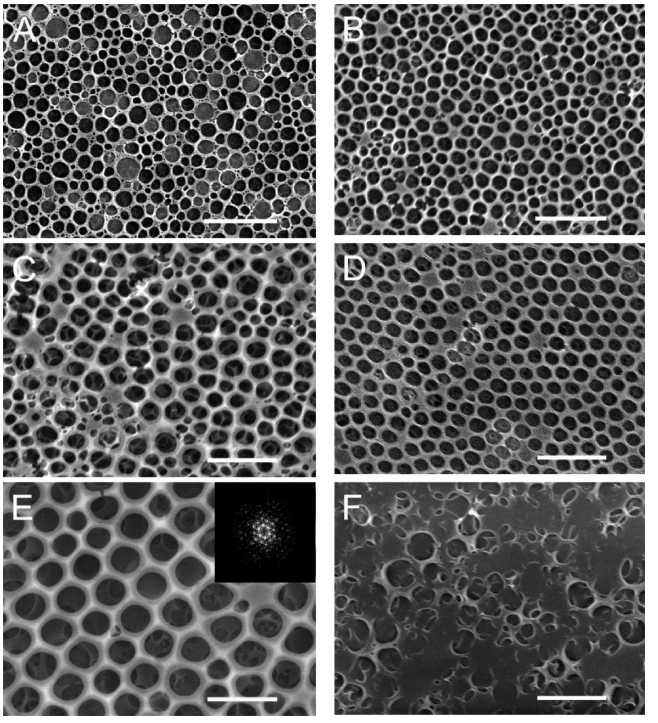

Figure 3. SEM images of honeycomb-structured BF films drop-cast on pristine silicon wafer for the triblock C6 with $CHCl_3$ solvent under various polymer concentrations of (A) 0.05, (B) 0.10v, (C) 0.20, (D) 0.40, (E) 0.80 (inset: FFT of the SEM image), and (F) 1.60% w/v at 47 RH% and 25 °C. Scale bar is 5 μm.

with less regularity and average pore size of $0.9 \pm 0.3\,\mu$m, and this maybe stem from inefficient encapsulation and stabilization of the condensed water-droplets levitating on the interface due to too low viscosity of amphiphile solution. When the polymer mass concentration increased from 0.10 to 0.80% w/v, multilayered microporous surfaces could be observed with increased average micropore sizes, and the pore distribution tended to be closer to regular hexagonal alignment. Furthermore, average pore sizes of the C6 films drop-cast under 0.10, 0.20, 0.40, and 0.80 w/v were further evaluated to be 0.9 ± 0.2, 1.1 ± 0.3, 1.2 ± 0.1, and $2.1 \pm 0.3\,\mu$m, respectively, and a fast Fourier-transformed (FFT) picture of original SEM image as shown as the inset of figure 3E indicated well-ordered distribution of surface micropores in the resulted BF film drop-cast under 0.80 *w/v*. In addition, the detected multilayered topologies could be accordingly interpreted for the submergence of fully stabilized water-droplets.[19] With regard to the influence of an amphiphile mass concentration on BF film formation, according to Pitois and Francois's study,[61] during drop-casting, the water-droplet radius (R) was proportional to the difference in temperature (ΔT) between the atmosphere and solution surface, and water-droplet growth time (t) as

$$R \sim (\Delta T^{0.8} t)^{1/3}$$

When increasing the amphiphile mass concentration of casting solution, the evaporation of volatile solvent would slow down due to the increased solution viscosity, and the ΔT would correspondingly decrease, whereas water-droplet growth time (t) would be elongated. The final water-droplet radius (R) would be determined by the both factors, which vary oppositely with amphiphile mass concentration. Commonly, ΔT has been known to be the predominant factor in regulating average pore sizes of BF films, and an increased mass concentration of drop-casting solution would generally lead to smaller pores. In contrast, except for the surface topology drop-cast under 1.60% w/v (Figure 3F), the average pore sizes in Figure 3 tended to increase with the amphiphile C6 mass concentration, implying that the elongated droplet growth time (t) hereby became the major factor, and resulted in larger size droplets by uptake of moisture and possible water-droplet coalescence.

As for the drop-casting parameters of humidity, Figure 4 depicts the SEM surface topologies for the amphiphile C6 cast on silicon wafer at 35 °C under various humid atmospheres. It could be seen that honeycomb-like surface morphology formed with better order under 40 RH%, and a higher humidity applied during drop-casting tended to result in less-ordered topologies and increased surface roughness for the amphiphile C6 BF films. Furthermore, the surface topology and roughness of the C6 BF films drop-cast under different humidity were analyzed by AFM as shown in Figure S3 in the Supporting Information. It could be seen that the resulted AFM surface topologies were in well agreement with those results by SEM, and surface roughness parameters R_q (root-mean square deviation) and R_a (arithmetic average deviation) of BF films drop-cast under 50−70 RH% (R_q = 179.4−306.0 nm, R_a = 144.2−238.4 nm) were 1.1−2.6 times higher than those BF films cast under 40 RH% (R_q = 84.3 nm, R_a = 67.3 nm) as shown in Figure 5.

Alternatively, the drop-casting substrate also seems to influence the surface morphology of achieved BF thin film, and few works have been reported hitherto.[31,65,66] Figure S4 in the Supporting Information depicts SEM surface topologies for the

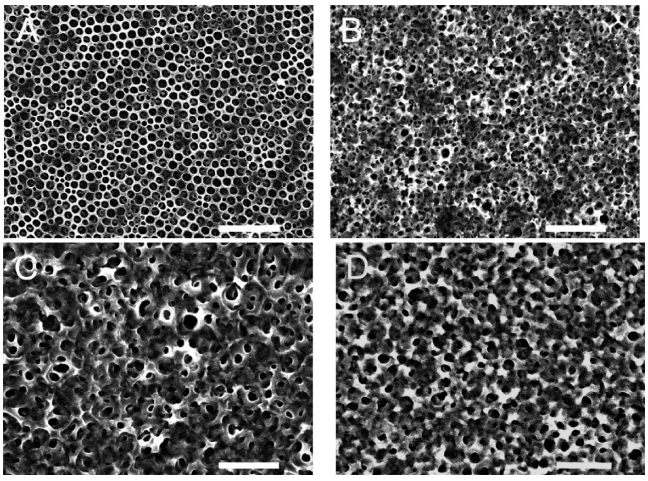

Figure 4. SEM images of the BF films drop-cast at 35 °C on pristine silicon wafer for the triblock C6 dissolved in $CHCl_3$ (0.40% w/v) under (A) 40, (B) 50, (C) 60, and (D) 70 RH%. Scale bar is 10 μm.

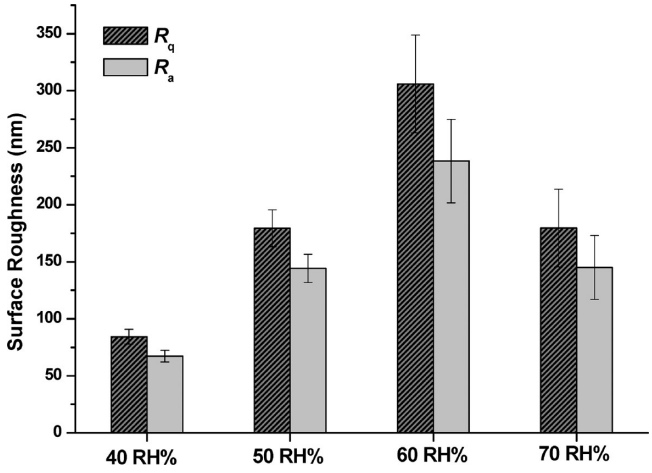

Figure 5. Surface roughness parameters R_q and R_a of the BF films drop-cast at 35 °C on pristine silicon wafer for the triblock C6 dissolved in $CHCl_3$ (0.40% w/v) under various concentrations. Data were calculated by AFM, and were shown as mean ± SD (n = 5).

C6 BF films drop-cast at 35 °C under 40 RH% and 0.40% w/v amphiphile mass concentration on different solid substrates of pristine silicon and the silicon substrates preliminarily dealt with hydrophilic and lipophilic organics (see the Supporting Information). Table 2 summarized the values of surface energy for the pristine and surface-modified silicon substrates, and a remarkably increased surface energy of 74.2 mN/m was found for the hydrophilic silicon substrate while the lipophilic silicon substrate showed a surface energy of 35.9 mN/m slightly lower than that of the pristine silicon substrate. After drop-casting the amphiphile C6 solution, average pore sizes of the achieved BF surfaces were calculated to be 1.3 ± 0.2, 1.6 ± 0.2, and $2.1 \pm 0.3\,\mu$m, respectively, and a lower surface energy of casting substrate interestingly tended to result in larger average micropore size of the formed BF film. Regarding the effect of substrate surface energy on drop-casting BF films, it could be anticipated that the multilayered film morphology might be associated with thermocapillary effect and Marangoni convection, and the different natures of

Table 2. Average Pore Sizes of Honeycomb-Structured BF Films for the Triblock C6 Drop-Cast on Silicon Wafers with Different Surface Energy

BF casting substrate	contact angle (water)[a]	contact angle (ethylene glycol)[a]	surface energy (mN/m)[b]	average pore size (μm)[c]
clean silicon wafer	68.0	33.3	40.8	1.6 ± 0.2
hydrophilic silicon wafer	32.6	31.9	74.2	1.3 ± 0.2
hydrophobic silicon wafer	84.6	52.1	35.9	2.1 ± 0.3

Notes: [a] Determined by Drop Shape analysis software (Kruess, Germany) based on the images of liquid droplets taken every 5 s for 30 s since dropped on substrates. [b] Calculated according to the Owens−Wendt−Rabel−Kaelble method by Drop Shape analysis software. [c] Calculated by ImageJ software (Wayne Rasband, USA) based on SEM images.

substrate surface may give rise to different interactions between substrate surface and drop-casting solution, and finally lead to different sizes of formed micropores.

In addition, the influences of drop-casting temperature on surface topologies of BF films were also examined, since temperature strongly affected the solvent evaporation rate and partial pressures of water vapor p. The partial pressures of water vapor p were accordingly evaluated as

$$p = p_s \times \mathrm{RH}\%$$

where p_s means the saturation vapor pressure at a given temperature.[67] As shown in Figure S5 in the Supporting Information, similar honeycomb-structured surface topologies were observed when the C6 BF films were drop-cast at 25 and 35 °C under 47 RH% with corresponding partial pressure of water vapor p equal to 1.49×10^3 and 2.64×10^3 Pa, respectively. It seems that a higher drop-casting temperature led to faster evaporation of volatile solvent, larger temperature gradient and more intense convection in the amphiphile C6 solution on the substrate surface, and this consequently resulted in a larger number of micropores in the underlayers (see Figure S5B in the Supporting Information). Moreover, when the amphiphile C6 solution drop-cast at a high temperature of 45 or 55 °C under 47 RH% with partial pressure of water vapor p equal to 4.51×10^3 and 7.40×10^3 Pa, respectively, nonporous flat surface topologies of BF films were observed in Figure S5 in the Supporting Information, and this result may be accounted for too fast evaporation of organic solvent and possible decreased molecular hydrophilicity of the amphiphile C6 under a higher temperature.

Cytotoxicity and Cell Growth with Microporous Surface Amphiphile Films As the Scaffolds. Recently, the porous substrates with greatly enlarged surface area have been becoming interesting, and emerged as a new type of multidimensional scaffolds for tissue engineering and regeneration,[18] and the porous polymer films with patterned arrays and tunable pore sizes by facile BF method made it possible to investigate the effect of scaffold surface structures on cell growth and proliferation.[18−20,68] In this work, cell toxicity of honeycomb-like films by amphiphile C6 drop-cast at 35 °C, 47 RH% and 0.40% w/v with CH_2Cl_2 or $CHCl_3$ solvent was examined with MTT assay and HeLa cells, and the results shown in figure 6 with pristine silicon as the control

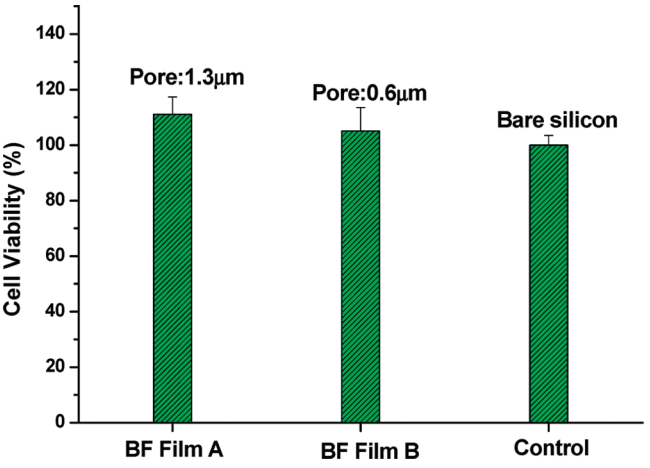

Figure 6. Cell viability of the honeycomb-structured BF films for the triblock C6 drop-cast on pristine silicon wafer with different solvents of (A) $CHCl_3$ and (B) CH_2Cl_2 at amphiphile concentration of 0.40% w/v under 35 °C and 40 RH% with bare silicon wafer as the control, and data were shown as the mean + SD (n = 3).

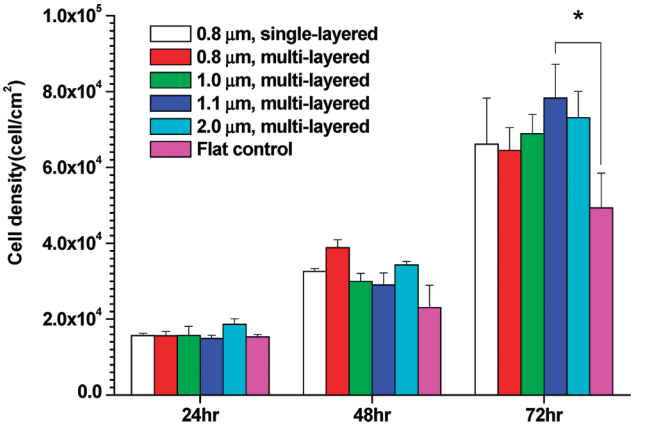

Figure 7. Incubation time dependence of HeLa cell density on the honeycomb-structured BF films for the triblock C6 with different average pore sizes and the spin-coated flat control. Results are expressed as mean + SD (n = 3), *p < 0.05 when the group was compared with flat films using Student's t test.

clearly indicated slight enhancement of cell growth on the honeycomb-like microporous films and low cell toxicity of the amphiphile C6. Meanwhile, with the microporous films as cell scaffolds, the film surface structure dependence of HeLa cell growth and proliferation was further investigated, and microscopic pictures of living HeLa cells were recorded as shown in Figure S6 in the Supporting Information, and their cell densities on scaffold surface were further evaluated as shown in Figure 7. It could be seen that after 24 h cell cultivation, no remarkable difference in HeLa cell density (1.53×10^4 to 1.86×10^4 cells/cm^2) was observed between the honeycomb-like films and the flat control, and 48 h later cell densities of the porous C6 films with microporous topologies (2.90×10^4 to 3.89×10^4 cells/cm^2) became slightly higher than that of the flat control. Intriguingly, after 72 h of incubation, the honeycomb-like C6 substrates showed obviously enhanced cell densities (6.45×10^4 to 7.83×10^4 cells/cm^2) as compared to that of a flat control (4.93×10^4 cells/cm^2).

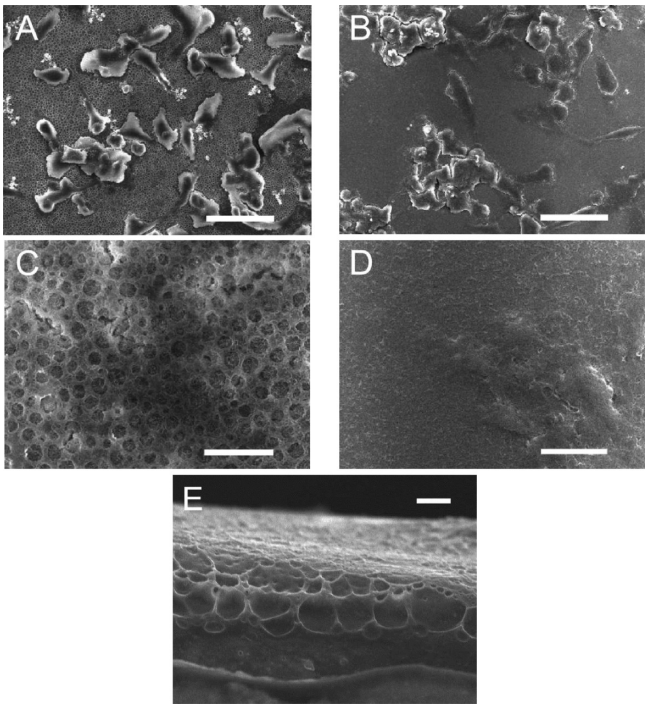

Figure 8. SEM images of HeLa cells after 72 h of cell cultivation and fixation on the drop-cast honeycomb-structured BF films of (A) the triblock C6, (B) its spin-coated flat film control (scale bar is 50 μm), (C) enlarged surface topologies of the honeycomb-structured BF film and (D) the flat control and (E) cross-section view of the microporous BF film (scale bar is 5 μm).

In addition, as seen figure 7, a statistically significant difference ($p < 0.05$, Student's t test) of HeLa cell densities between microporous BF films with pore size of ~1.1 μm and flat surface films was observed after 72 h cell cultivation. Moreover, figure 8 shows the fixed cells on the honeycomb structured C6 substrate (A) and a C6 flat control (B) after 72-h cell cultivation, and a more uniform cell distribution and better adhesion could be observed on the C6 BF substrate surface.The 3D-structured substrates, as indicated by the SEM cross-section view of BF films shown in Figure 8E, seem to be close to real status for cell adhesion and proliferation in vivo, and the microporous surface may be favorable for supplying nutrients and greatly enlarged surfaces. In particular, a C6 film with well-ordered micropores at the BF film surface showed a lower water-contact angle than that of the film with irregular coarse surface as shown in Figure S7 in the Supporting Information, and the lower contact angle would be favorable for apparent cell attachment and proliferation. In fact, the mechanism concerning the enhanced cell growth on the substrates with ordered BF arrays and possible cell/interface interactions still kept not so clear yet, and the honeycomb-like thin films by the new amphiphile C6 comprising PLLA and L-lysine dendron seem to be a favorable system for exploring the effects of micropore and multilayered structures at different length scales on cell growth behavior and the interaction between cell and interface. In particular, a plenty of free amino functional groups at the porous surface of triblock dendritic poly(L-lysine)-*b*-poly(L-lactide)-*b*-dendritic poly(L-lysine) BF films may further provide new possibility for attaching diverse bioactive compounds toward biological application, and these are now under investigation in this lab.

CONCLUSIONS

In this study, two new series of multifunctional amphiphilic copolymers of diblock DL_1-$PLLA_{18.7}$, DL_2-$PLLA_{16.6}$, DL_3-$PLLA_{18.7}$, and triblock DL_1-$PLLA_{12.0}$-DL_1, DL_1-$PLLA_{16.1}$-DL_1, DL_1-$PLLA_{37.7}$-DL_1(C1−C6) bearing well-defined structures were synthesized with various PLLA hydrophobic block lengths and hydrophilic L-lysine dendritic generations. Through a static BF fabrication method, honeycomb-structured microporous films of the prepared amphiphiles were drop-cast, and successfully achieved with ordered BF arrays, and their averaged micropore diameter size and ordered surface topologies of the BF films were found to strongly depend on the hydrophilic/hydrophobic block molar ratio and molecular architecture of amphiphiles as well as the drop-casting parameters of amphiphile concentration, temperature and humidity. It was found that a higher amphiphile concentration, a lower drop-casting temperature and a lower humidity consequently tended to self-assemble larger size micropore arrays with more perfectly ordered alignment. It was also interestingly revealed that for the amphiphile C6, the micropore sizes of honeycomb-structured BF films remarkably depended on surface energy of the drop-casting substrates, and a more hydrophilic substrate surface tended to form smaller size micropores of BF arrays. Furthermore, MTT assay with HeLa cells demonstrated very low cytotoxicity for the prepared honeycomb-structured microporous films, and compared to 2D flat control, the new functional 3D scaffolds showed obvious enhancement of HeLa cell proliferation.

Since the surface micropore sizes and layered structures of self-assembled BF arrays can be readily tuned for these biodegradable linear−dendritic amphiphiles, and hydrophilic L-lysine dendrons at the pore interfaces bear abundant amino functionalities, therefore these ordered honeycomb-structures might provide new multidimensional scaffold materials for potential biomedical application and biological separation, and further studies are now under investigation in this lab.

ASSOCIATED CONTENT

Supporting Information. Silicon wafer treatment, ^{1}H NMR spectra for S1−S3 and S6 in $CDCl_3$, MALDI-MS spectrum for C6, AFM images of the BF films drop-cast at 35 °C on pristine silicon wafer for C6 solution in $CHCl_3$ under various RH%, SEM images of the honeycomb-structured BF films for C6 solution in $CHCl_3$ drop-cast on silicon substrates with different surface energy, SEM images of films prepared by drop-casting on silicon wafer for C6 solution in $CHCl_3$ at different temperatures, optical micrographs of HeLa cells on honeycomb-structured amphiphile C6 BF films and the flat control, SEM images and water contact angle test results of films prepared by drop-casting on silicon wafer for the C6 solution in various RH% (PDF). This material is available free of charge via the Internet at http://pubs.acs.org.

AUTHOR INFORMATION

Corresponding Author

*Phone & fax: +86-21-5492-5303. E-mail: acao@mail.sioc.ac.cn.

ACKNOWLEDGMENT

The authors are indebted to the financial supports partially from national science foundation of China (20874114, 21002116), science and technology commission of Shanghai municipality

(10QH1403000, 10R21418400), and China postdoctoral foundation council (20090460676).

REFERENCES

(1) Menard, E.; Meitl, M. A.; Sun, Y.; Park, J.-U.; Shir, D. J.-L.; Nam, Y.-S.; Jeon, S.; Rogers, J. A. *Chem. Rev.* **2007**, *107*, 1117–1160.

(2) Geissler, M.; Xia, Y. *Adv. Mater.* **2004**, *16*, 1249–1269.

(3) DeRosa, C.; Park, C.; Thomas, E. L.; Lotz, B. *Nature* **2000**, *405*, 433–437.

(4) Erdogan, B.; Song, L.; Wilson, J. N.; Park, J. O.; Srinivasarao, M.; Bunz, U. H. F. *J. Am. Chem. Soc.* **2004**, *126*, 3678–3679.

(5) Yunus, S.; Spano, F.; Patrinoiu, G.; Bolognesi, A.; Botta, C.; Brühwiler, D.; Ruiz, A. Z.; Calzaferri, G. *Adv. Funct. Mater.* **2006**, *16*, 2213–2217.

(6) Si, H.-Y.; Yuan, D.; Chen, J.-S.; Chow, G.-M.; Zhang, H.-L. *J. Colloid Interface Sci.* **2011**, *353*, 569–573.

(7) Tanev, P. T.; CFHibwe, M.; Pinnavala, T. J. *Nature* **1994**, *368*, 321–323.

(8) Ma, H.; Cui, J.; Chen, J.; Hao, J. *Chem.—Eur. J.* **2011**, *17*, 655–660.

(9) Kim, J.; Serpe, M. J.; Lyon, L. A. *Angew. Chem., Int. Ed.* **2005**, *44*, 1333–1336.

(10) Yabu, H.; Takebayashi, M.; Tanaka, M.; Shimomura, M. *Langmuir* **2005**, *21*, 3235–3237.

(11) Ting, W.-H.; Chen, C.-C.; Dai, S. A.; Suen, S.-Y.; Yang, I.-K.; Liu, Y.-L.; Chen, F. M. C.; Jeng, R.-J. *J. Mater. Chem.* **2009**, *19*, 4819–4828.

(12) Lu, X.; Zhang, C.; Han, Y. *Macromol. Rapid Commun.* **2004**, *25*, 1606–1610.

(13) Tanaka, M.; Takebayashi, M.; Miyama, M.; Nishida, J.; Shimomura, M. *Biomed. Mater. Eng.* **2004**, *14*, 439–446.

(14) Zhang, Y.; Wang, C. *Adv. Mater.* **2007**, *19*, 913–916.

(15) Min, E.; Wong, K. H.; Stenzel, M. H. *Adv. Mater.* **2008**, *20*, 3550–3556.

(16) Ke, B.-B.; Wan, L.-S.; Xu, Z.-K. *Langmuir* **2010**, *26*, 8946–8952.

(17) Sunami, H.; Ito, E.; Tanaka, M.; Yamamoto, S.; Shimomura, M. *Colloids Surf., A* **2006**, *284−285*, 548–551.

(18) Beattie, D.; Wong, K. H.; Williams, C.; Poole-Warren, L. A.; Davis, T. P.; Barner-Kowollik, C.; Stenzel, M. H. *Biomacromolecules* **2006**, *7*, 1072–1082.

(19) Li, L.; Chen, C.; Li, J.; Zhang, A.; Liu, X.; Xu, B.; Gao, S.; Jin, G.; Ma, Z. *J. Mater. Chem.* **2009**, *19*, 2789–2796.

(20) Nishikawa, T.; Ookura, R.; Nishida, J.; Arai, K.; Hayashi, J.; Kurono, N.; Sawadaishi, T.; Hara, M.; Shimomura, M. *Langmuir* **2002**, *18*, 5734–5740.

(21) Choi, S.-W.; Xie, J.; Xia, Y. *Adv. Mater.* **2009**, *21*, 2997–3001.

(22) Yamamoto, S.; Tanaka, M.; Sunami, H.; Ito, E.; Yamashita, S.; Morita, Y.; Shimomura, M. *Langmuir* **2007**, *23*, 8114–8120.

(23) Berry, C. C.; Dalby, M. J.; McCloy, D.; Affrossman, S. *Biomaterials* **2005**, *26*, 4985–4992.

(24) Fukuhira, Y.; Kitazono, E.; Hayashi, T.; Kaneko, H.; Tanaka, M.; Shimomura, M.; Sumi, Y. *Biomaterials* **2006**, *27*, 1797–1802.

(25) Li, L.; Li, J.; Zhong, Y.; Chen, C.; Ben, Y.; Gong, J.; Ma, Z. *J. Mater. Chem.* **2010**, *20*, 5446–5453.

(26) Sirbuly, D. J.; Lowman, G. M.; Scott, B.; Stucky, G. D.; Buratto, S. K. *Adv. Mater.* **2003**, *15*, 149–152.

(27) Bunz, U. H. F. *Adv. Mater.* **2006**, *18*, 973–989.

(28) Masuda, H.; Watanabe, M.; Yasui, K.; Tryk, D.; Rao, T.; Fujishima, A. *Adv. Mater.* **2000**, *12*, 444–447.

(29) Widawski, G.; Rawiso, M.; Francois, B. *Nature* **1994**, *369*, 387–387.

(30) Govor, L. V.; Bashmakov, I. A.; Kiebooms, R.; Dyakonov, V.; Parisi, J. *Adv. Mater.* **2001**, *13*, 588–591.

(31) Billon, L.; Manguian, M.; Pellerin, V.; Joubert, M.; Eterradossi, O.; Garay, H. *Macromolecules* **2009**, *42*, 345–356.

(32) Ghannam, L.; Manguian, M.; Francois, J.; Billon, L. *Soft Matter* **2007**, *3*, 1492–1499.

(33) Stenzel, M. H.; Barner-Kowollik, C.; Davis, T. P. *J. Polym. Sci., Part A: Polym. Chem.* **2006**, *44*, 2363–2375.

(34) Harada, A.; Kobayashi, R.; Takashima, Y.; Hashidzume, A.; Yamaguchi, H. *Nature Chem.* **2011**, *3*, 34–37.

(35) Percec, V.; Wilson, D. A.; Leowanawat, P.; Christopher, J, W.; Hughes, A. D.; Kaucher, M. S.; Hammer, D. A.; Levine, D. H.; Kim, A. J.; Bates, F. S.; P.Davis, K.; Lodge, T. P.; Klein, M. L.; DeVane, R. H.; Aqad, E.; Rosen, B. M.; Argintaru, A. O.; Sienkowska, M. J.; Rissanen, K.; Nummelin, S.; Ropponen, J. *Science* **2010**, *328*, 1009–1014.

(36) Li, L.; Zhong, Y.; Gong, J.; Li, J.; Chen, C.; Zenga, B.; Ma, Z. *Soft Matter* **2011**, *7*, 546–552.

(37) Li, L.; Zhong, Y.; Gong, J.; Li, J.; Huang, J.; Ma, Z. *J. Colloid Interface Sci.* **2011**, *354*, 758–764.

(38) Jiang, X.; Zhou, X.; Zhang, Y.; Zhang, T.; Guo, Z.; Gu, N. *Langmuir* **2010**, *26*, 2477–2483.

(39) Li, L.; Chen, C.; Zhang, A.; Liu, X.; Cui, K.; Huang, J.; Ma, Z.; Han, Z. *J. Colloid Interface Sci.* **2009**, *331*, 446–452.

(40) Kabuto, T.; Hashimoto, Y.; Karthaus, O. *Adv. Funct. Mater.* **2007**, *17*, 3569–3573.

(41) Liu, C.; Gao, C.; Yan, D. *Angew. Chem., Int. Ed.* **2007**, *46*, 4128–4131.

(42) Wong, K. H.; Stenzel, M. H.; Duvall, S.; Ladouceur, F. *Chem. Mater.* **2010**, *22*, 1878–1891.

(43) Connal, L. A.; Vestberg, R.; Hawker, C. J.; Qiao, G. G. *Adv. Funct. Mater.* **2008**, *18*, 3706–3714.

(44) Vamvounis, G.; Nystrom, D.; Antoni, P.; Lindgren, M.; Holdcroft, S.; Hult, A. *Langmuir* **2006**, *22*, 3959–3961.

(45) Song, L.; Bly, R. K.; Wilson, J. N.; Bakbak, S.; Park, J. O.; Srinivasarao, M.; Bunz, U. H. F. *Adv. Mater.* **2004**, *16*, 115–118.

(46) Englert, B. C.; Scholz, S.; Leech, P. J.; Srinivasarao, M.; Bunz, U. H. F. *Chem.—Eur. J.* **2005**, *11*, 995–1000.

(47) Connal, L. A.; Franks, G. V.; Qiao, G. G. *Langmuir* **2010**, *26*, 10397–10400.

(48) Hsu, J.-C.; Sugiyama, K.; Chiu, Y.-C.; Hirao, A.; Chen, W.-C. *Macromolecules* **2010**, *43*, 7145–7158.

(49) Kato, K.; Uchida, E.; Kang, E.-T.; Uyama, Y.; Ikada, Y. *Prog. Polym. Sci.* **2003**, *28*, 209–259.

(50) Burg, K. J. L.; Porter, S.; Kellam, J. F. *Biomaterials* **2000**, *21*, 2347–2359.

(51) Chaudhuri, J. B.; Davidson, M. G.; Ellis, M. J.; Jones, M. D.; Wu, X. *Macromol. Symp.* **2008**, *272*, 52–57.

(52) Zhao, B.; Zhang, J.; Wang, X.; Li, C. J. *Mater. Chem.* **2006**, *16*, 509–513.

(53) Servoli, E.; Ruffo, G. A.; Migliaresi, C. *Polymer* **2010**, *51*, 2337–2344.

(54) Fukuhira, Y.; Yabu, H.; Ijirod, K.; Shimomura, M. *Soft Matter* **2009**, *5*, 2037–2041.

(55) Tian, Y.; Ding, H.; Jiao, Q.; Shi, Y. *Macromol. Chem. Phys.* **2006**, *207*, 545–553.

(56) Li, Y.; Li, Q.; Li, F.; Zhang, H.; Jia, L.; Yu, J.; Fang, Q.; Cao, A. *Biomacromolecules* **2006**, *7*, 224–231.

(57) Li, Y.; Cui, L.; Li, Q.; Jia, L.; Xu, Y.; Fang, Q.; Cao, A. *Biomacromolecules* **2007**, *8*, 1409–1416.

(58) Li, Y.; Zhu, Y.; Xia, K.; Sheng, R.; Jia, L.; Hou, X.; Xu, Y.; Cao, A. *Biomacromolecules* **2009**, *10*, 2284–2293.

(59) Zhu, Y.; Sheng, R.; Luo, T.; Li, H.; Sun, W.; Li, Y.; Cao, A. *Macromol. Biosci.* **2011**, *11*, 174–186.

(60) Stenzel, M. H.; Davis, T. P. *Aust. J. Chem.* **2003**, *56*, 1035–1038.

(61) Pitois, O.; Francois, B. *Colloid Polym. Sci.* **1999**, *277*, 574–578.

(62) Srinivasarao, M.; Collings, D.; Philips, A.; Patel, S. *Science* **2001**, *292*, 79–83.

(63) Ke, B.-B.; Wan, L.-S.; Chen, P.-C.; Zhang, L.-Y.; Xu, Z.-K. *Langmuir* **2010**, *26*, 15982–15988.

(64) Wong, K. H.; Davis, T. P.; Barner-Kowollik, C.; Stenzel, M. H. *Polymer* **2007**, *48*, 4950–4965.

(65) Cheng, C. X.; Tian, Y.; Shi, Y. Q.; Tang, R. P.; Xi, F. *Langmuir* **2005**, *21*, 6576–6581.

(66) Ferrari, E.; Fabbri, P.; Pilati, P. *Langmuir* **2011**, *27*, 1874–1881.

(67) Perry, R. H; Green, D. W. *Perry's Chemical Engineers's Handbook*, 8th ed.; McGraw-Hill: New York, 2008; pp 12−4.

(68) Lee, S. J.; Choi, J. S.; Park, K. S.; Khang, G.; Lee, Y. M.; Lee, H. B. *Biomaterials* **2004**, *25*, 4699–4707.